



Conflict Detection and Separation Configuration Method Based on Uncertain Flight Trajectory

Xuanming REN¹, Xinmin TANG², Kang ZHANG³, Qixing LU⁴

Original Scientific Paper
Submitted: 12 June 2023
Accepted: 20 Nov. 2023

¹ renxuanming1@126.com, Nanjing University of Aeronautics and Astronautics

² Corresponding author, tangxinmin@nuaa.edu.cn, Civil Aviation University of China

³ 2440717230@qq.com, Nanjing University of Aeronautics and Astronautics

⁴ luqixing2007@nuaa.edu.cn, Nanjing University of Aeronautics and Astronautics



This work is licensed under a Creative Commons Attribution 4.0 International License.

Publisher:
Faculty of Transport and Traffic Sciences,
University of Zagreb

ABSTRACT

Aiming at two aircraft conflict scenario in the pre-tactical stage, by converting the uncertain flight trajectory of the target aircraft into a spatio-temporal trajectory under its performance constraints, a conflict detection model based on truncated normal distribution was proposed, and influencing factors affecting the overall conflict probability were analysed by numerical simulation. For the conflict scenario, nonlinear particle swarm optimisation (NPSO) algorithm was applied to solve the optimal separation configuration strategy for the ownship. The simulation results show that, in comparison to conventional PSO algorithm, the improved NPSO algorithm improves the optimal value by 14.88% and decreases the maximum velocity change by 19.84%. The simulation also shows that the algorithm can maintain the minimum interval requirements under different initial parameters, demonstrating its strong adaptability.

KEYWORDS

conflict detection; separation configuration; spatio-temporal trajectory; uncertain flight trajectory; nonlinear particle swarm optimisation.

1. INTRODUCTION

In the context of NextGen2020, the implementation of Trajectory-Based Operations (TBO) will involve the integration of diverse data into 4D flight trajectory. Instead of relying on conventional positional, altitude and velocity information present in the original Air Traffic Management (ATM) environment, TBO will leverage trajectory information. And the pilot will refer to the pre-defined 4D trajectory to perform flight missions. Thus, it becomes imperative to assign pilots safe and conflict-free four-dimensional trajectories during the pre-tactical phase [1]. However, incomplete waypoint information and uncertainties such as positioning errors introduce a certain level of uncertainty in the aircraft's position between waypoints, thereby increasing the potential for conflicts [2]. Hence, the study of aircraft separation management under conditions of state uncertainty becomes an indispensable concern. Over the past decade, research on aircraft separation management has mainly focused on two aspects: conflict detection models and separation retention algorithms.

Flight conflict detection models can be divided into classical geometric models [5, 6] and probabilistic models [3, 4]. Geometric conflict detection has high requirements on the accuracy of information [5], and cannot take the uncertainty of the aircraft into consideration, so it has clear limitations. The probabilistic conflict detection of the aircraft is affected by internal and external uncertain factors such as wind field and pilot operation during the normal flight process, and the separation between any two aircraft is regarded as a random variable obeying a certain distribution function [7], which greatly improves the robustness and applicability of the reference trajectory in extreme cases.

In the case of the flight intention of target aircraft is known, because of the flight path has already been decided, the experts' research mainly focus on the uncertain impact of wind forecast errors and navigation errors. Eulalia et al. [8] modelled the wind component as a random variable obeying the beta distribution and used the Monte Carlo [9, 10] method for simulation verification. However, the calculation process of the Monte Carlo method is complicated, resulting in an excessive amount of calculation. Liu et al. [11] comprehensively considered the navigation error, control error, wind disturbance and other uncertain factors, and established a reasonable error model to calculate the instantaneous collision probability of aircraft in a short period of time. Alizadeh et al. [12] investigates the impact of wind uncertainty and the potential fuel-saving benefits through simulation analysis when precise wind force data is available. Lucas et al. [13] employed a sophisticated NoSQL database scheme to devise a Conflict Detection and Resolution (CD&R) framework for the management of four-dimensional trajectory navigation. Liu [14] synthesised Traffic Flow Management (TFM) and CD&R, and analysed the synergistic effects of TFM and CDR through random numerical experiments in high-density airspace scenarios. For scenarios where flight intention is unknown, experts build an intention model based on horizontal trajectory, altitude profiles and velocity profiles by analysing surveillance data such as radar [15], ADS-B [16, 17], and extrapolated the future flight trajectory of target aircrafts. In addition, by establishing a dynamic model [18] for the target aircraft, the experts convert the flight intention into a reachable space of the target aircraft, such as the conical reachable domain [19, 20], space-time prism (STP) [21]. And the conflict probability is calculated according to the size of the spatial intersection region.

Taken together, the current aircraft conflict detection studies fall into two main categories: one assumes that the aircraft follows a pre-determined trajectory exactly, and the other is based on the current or historical flight status of the aircraft and extrapolates the trajectory of the aircraft over a period of time in the future, which lacks the study of uncertain trajectories between two determined waypoints. In addition, the above studies mostly used instantaneous conflict to estimate the maximum conflict probability, which can only reflect the conflict possibility between aircraft at a certain moment, but not the comprehensive conflict probability among aircraft in a period of time and space. This may lead to the problem of false alert and missing alert when the maximum instantaneous conflict probability is used as the conflict detection index.

In terms of the separation assurance algorithm, the current mainstream optimal control algorithm is based on meta heuristic methods, such as neural network [22, 23], ant colony algorithm [24] and particle swarm optimisation (PSO) algorithm [25, 26]. Since optimal control problems for continuous systems can be hard to resolve, discretising the control variables can transform continuous problems into discrete problems that are much simpler to resolve. Omer et al. [27] discretised the continuous time variables and used the better feasible solution obtained by the mixed integer linear programming method as the initial value of the nonlinear model, which greatly boosted the algorithm's calculation accuracy, but at the same time reduced the solution efficiency. Recently, a method that discretises the range of heading angle has been used, which converts the nonlinear problem into a mixed integer linear programming problem [28], and the simulation results indicate that the compute speed can be markedly improved, but it is difficult to get the result of the local optimal solution. Matsuno et al. [29] established a three-dimensional conflict resolution model and proposed an algorithm that combines chaotic generalised polynomial and pseudo spectral methods. He then solved the conflict resolution problem as a random optimal control problem, which greatly improved the calculation efficiency, but was also confronted with the problem of local optimal solution. Emami et al. [30] argues that the particle swarm optimisation (PSO) algorithm has advantages in solving flight conflict problems due to its ability to optimise particle velocity and position. The author compares the PSO algorithm with other commonly used optimisation algorithms [31], discusses multi-agent flight conflict problems and conducts simulations for five common conflict scenarios. The simulation results demonstrate that the PSO algorithm outperforms the compared algorithms in terms of computation time and optimal values. In addition, there are other separation control methods, exemplified by the utilisation of Markov decision trees to ascertain conflict-free control sequences under uncertain aircraft states [13]. It is noteworthy that these

methods are exclusively applicable in the pursuit of suboptimal solutions. Another avenue involves the derivation of conflict-free trajectories through the application of geometric and physical principles, relying on aircraft waypoints information gleaned from airborne surveillance system [5, 6]. Nevertheless, it is imperative to acknowledge that the assumptions requisite for the viability of such methods are excessively stringent.

To address potential flight conflict issues arising from uncertainties, we explored a scenario of dual-aircraft following conflict at pre-tactical stage, wherein the 3D trajectories (longitude, latitude and time) of the two planes exhibit overlapping regions. We have developed a conflict detection model that transforms the uncertain flight state of the target aircraft between waypoints into a spatiotemporal trajectory constrained by aircraft performance. This model enables us to identify the conflict risk of our aircraft within conflict segments. Building upon the notion of space-time prism, we have employed the truncated normal distribution to effectively detect potential conflicts among aircraft, adopt the particle swarm optimisation algorithm to enforce separation control for aircraft flagged as being in conflict. In summary, the pre-tactical trajectory calculated in this study can reduce unnecessary tactical manoeuvres, thereby providing a theoretical foundation for future air traffic technologies based on TBO operation.

2. AIRCRAFT POSITION PREDICTION MODEL

The airway, the air traffic control and airdrome collaborate to create a flight plan that details the ETA of the waypoints during the pre-tactical stage of an aircraft mission. However, there is uncertainty in the route of aircraft between waypoints due to incomplete ETA information or airspace control variables, particularly when two waypoints are far apart. The flying safety between aircrafts will be significantly impacted by this ambiguity. As a result, in this study, we take into account creating a reachable domain model of target aircraft without changing the flight altitude during the cruise phase, identifying the risk of a conflict based on a truncated normal distribution. Finally, the separation control is implemented according to the PSO algorithm for the possible conflict scenarios of the aircraft.

2.1 Kinematics model of ownship

This study deals with the conflict detection and interval reconfiguration ability of aircraft in cruise phase. Based on that, in this work we ignore the separation assurance strategies in vertical direction, and only discuss the adjustment strategies in horizontal direction. As shown in *Figure 1*, the aircraft motion model of ownship A and target aircraft B in the same flight segment is established based on the two-dimensional coordinate system. At the initial moment, both ownship A and target aircraft B flight at a constant speed along the X-axis, V_0^A and V_0^B are initial velocity, respectively. The conflict protection domain is a circular area, the centre of which is the ownship and the radius is r_A . As a result, this manuscript aims to meticulously construct a reachable domain model for the target aircraft, while concurrently maintaining the flight altitude unaltered during the cruise phase. By leveraging the truncated normal distribution, we discern the potential hazards of conflicts with utmost precision.

During the course of actual flight operations, aircraft typically navigate along a four-dimensional trajectory composed of a series of waypoints and estimated time of arrival (ETA) as defined in the flight plan [32].

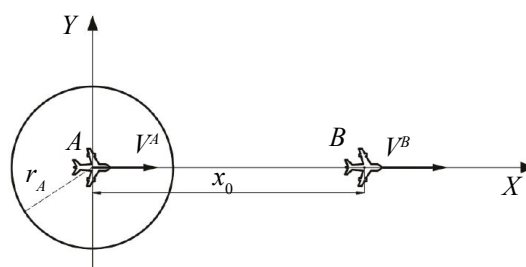


Figure 1 – Following model of aircraft

However, the aircraft may not always have access to the ETA of the target aircraft. Additionally, the human factors of pilots can also cause uncertainty in flight state, leading to potential conflicts in the spatiotemporal trajectories between aircraft.

2.2 Reachable domain model of target aircraft

Due to the ability of Brownian motion to describe the complexity and uncertainty of aircraft motion, and to provide a probabilistic description of aircraft motion, the possible position of the aircraft can be predicted by calculating the probability density function. Furthermore, despite the stochastic nature of Brownian motion, it exhibits determinism and predictability on larger time scales, thereby enhancing the accuracy of flight conflict prediction. Consequently, this study adopts the assumption that aircraft motion follows Brownian motion in order to address the challenges of flight conflict arising from inherent uncertainties. Assuming that the position probability of target aircraft in the reachable region can be expressed by truncated normal distribution. In addition, to ensure the rationality of the motion model and the conflict detection model, we made the following assumptions:

- 1) The two aircraft proceed according to their individual flight plan, wherein their trajectories exhibit a region of the overlapping area.
- 2) To simplify the model, the aircraft will not change its altitude because civil aircraft usually fly at the same altitude in the cruise phase.
- 3) The ETA of the start point is a fixed value, so as to stick out the principle and calculation process of the decision-making scheme.

Since the independent influence of uncertainty interference on the longitudinal and lateral speeds of target aircraft is independent, the motion model of the target aircraft between waypoints $X_{B1}(x_1,y_1)$ and $X_{B2}(x_2,y_2)$ is established in this study, which is shown in Figure 2.

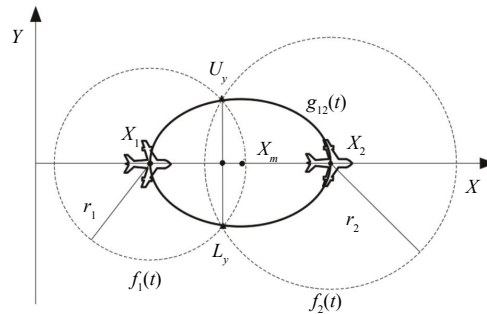


Figure 2 – Schematic diagram of the traffic aircraft motion model

In Figure 2, $f_1(t)$ and $f_2(t)$ represent the reachable range of target aircraft at waypoints X_{B1} and X_{B2} , respectively. The expressions are as follows:

$$f_1(t) = \{(x,y) | \sqrt{|x-x_1|^2 + |y-y_1|^2} \leq r_1\} \tag{1}$$

$$f_2(t) = \{(x,y) | \sqrt{|x-x_2|^2 + |y-y_2|^2} \leq r_2\} \tag{2}$$

$$\begin{cases} r_1 = (t-t_s) \cdot V_{max}^A \\ r_2 = (t-t) \cdot V_{max}^A \\ t_s \leq t \leq t_t \end{cases} \tag{3}$$

Here V_m^A indicates the maximum flight airspeed of target aircraft; t is the current moment when target moves between X_{B1} and X_{B2} ; t_s denotes the moment when target aircraft arrive at initial point X_{B1} , which takes the value of 0; and t_t defines the moment when target aircraft arrive at end point X_{B2} , which is uncertain. Considering the relatively stable airspeed of the aircraft during cruise phase, we presume that the mean velocity \bar{V} of the aircraft between two waypoints is as follows:

$$\bar{V} = V_0^B + w \tag{4}$$

Where, V_0^B is the velocity when target aircraft is at start point X_{B1} , $w \sim (0, \delta)$ represents the uncertainty interference term. Consequently, we can deduce that the temporal of the aircraft arrival at terminal point is as follows:

$$t_t = \frac{x_2 - x_1}{\bar{V}} \tag{5}$$

The expression for the coordinates of the midpoint of the flight segment is given as Equation 6:

$$X_m = \left(\frac{x_1 + x_2}{2}, \frac{y_1 + y_2}{2} \right) \tag{6}$$

Centre distance:

$$R_{12} = \sqrt{(x_2 - x_1)^2 + (y_2 - y_1)^2} \tag{7}$$

To succinctly convey the intersection point of the reachable domain of the target at endpoint $f_1(t)$ and $f_2(t)$, it is necessary to build a new coordinate system. Let two orthogonal unit vectors \bar{a} and \bar{b} be the new coordinate axes of X and Y, and the origin is the midpoint X_m , then the new coordinate system M is as follows:

$$\bar{a} = \left(\frac{x_2 - x_1}{R_{12}}, \frac{y_2 - y_1}{R_{12}} \right), \bar{b} = \left(\frac{y_2 - y_1}{R_{12}}, -\frac{x_2 - x_1}{R_{12}} \right) \tag{8}$$

In the new coordinate system M, the reachable range equations were changed as follows:

$$f_1(t) = \{(a, b) | (a + R_{12}/2)^2 + b^2 \leq r_1^2\} \tag{9}$$

$$f_2(t) = \{(a, b) | (a - R_{12}/2)^2 + b^2 \leq r_2^2\} \tag{10}$$

Thus, the intersection coordinates $U_y(a, b_1)$, $L_y(a, b_2)$ in the M coordinate system are determined by Equation 9 and Equation 10:

$$a = \frac{r_1^2 - r_2^2}{2R_{12}}, b_{1,2} = \pm \sqrt{\frac{r_1^2 - r_2^2}{2R_{12}} - \frac{(r_1^2 - r_2^2)^2}{4R_{12}^2} - \frac{R_{12}^2}{4}} \tag{11}$$

Finally, convert the coordinate system M to the original coordinate system to obtain the coordinates of the intersection point $U_y(u_x, u_y)$, $L_y(l_x, l_y)$:

$$\begin{aligned} U_y(u_x, u_y) &= \\ &= \frac{1}{2}(x_1 + x_2, y_1 + y_2) + \frac{r_1^2 - r_2^2}{2R_{12}^2}(x_2 - x_1, y_2 - y_1) + \frac{1}{2} \sqrt{2 \frac{r_1^2 + r_2^2}{2R_{12}^2} - \frac{(r_1^2 - r_2^2)^2}{R_{12}^4} - 1} (y_2 - y_1, x_2 - x_1) \end{aligned} \tag{12}$$

$$\begin{aligned} L_y(l_x, l_y) &= \\ &= \frac{1}{2}(x_1 + x_2, y_1 + y_2) + \frac{r_1^2 - r_2^2}{2R_{12}^2}(x_2 - x_1, y_2 - y_1) - \frac{1}{2} \sqrt{2 \frac{r_1^2 + r_2^2}{2R_{12}^2} - \frac{(r_1^2 - r_2^2)^2}{R_{12}^4} - 1} (y_2 - y_1, x_2 - x_1) \end{aligned} \tag{13}$$

According to the definition of the ellipse expression, the reachable domain $g_{12}(t)$ of the target aircraft from waypoint X_{B1} to X_{B2} at time t can be described as the following equations:

$$\sqrt{(2x - x_1 - x_2)^2 + \frac{4y^2 u_y^2}{(u_x - x_1)(x_2 - u_x)}} \leq 2R_{12} \tag{14}$$

2.3 Position prediction of the target aircraft

After obtaining the instantaneous reachable domain of the target, we use a STP to delineate the target’s reachable domain over the entire temporal realm. As to the time-varying characteristics of the STP, we apply the truncated normal distribution to predict the time-varying reachable domain of the target aircraft, which is limited to the dynamic spatial range of Figure 3.

As shown in Figure 3, waypoints X_{B1} and X_{B2} of the STP of target aircraft in the reachable domain of other machines can be expressed as $(\bar{V}(t_1 - t), 0)$ and $(\bar{V}(t_2 - t), 0)$, and the general formula of the truncated probability distribution [17] is as follows:

$$\left\{ \begin{aligned} Pr(x) = f(x | x_{min} < x < x_{max}) &= \frac{\varphi(x)}{\phi(x_{max}) - \phi(x_{min})} \\ \phi(x) &= \int_{-\infty}^x \varphi(x) dx \\ \varphi(x) &= \frac{1}{\sqrt{2\pi} \cdot \sigma} e^{-\frac{(x-u)^2}{2\sigma^2}} \end{aligned} \right. \quad (15)$$

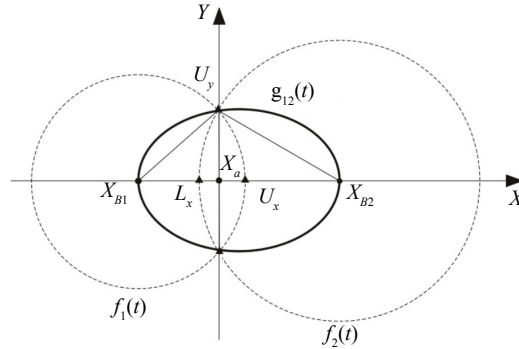


Figure 3 – Time based truncated probability distribution

Equation 15 indicates the truncated probability distribution Pr of the random variable x , which is distributed according to the probability density function $\varphi(x)$ and the cumulative density function $\phi(x)$. Then the probability density function of the lateral coordinate $X(t)$ of the target aircraft obeying the truncated probability distribution Pr_x with time t is as follows:

$$Pr_x(X(t)) \sim \frac{N(u_x, \sigma_x^2(t))}{\phi(U_x(t)) - \phi(L_x(t))} \quad (16)$$

$$L_x(t) = (\bar{V} - V_m) \cdot (t_t - t) \quad (17)$$

$$U_x(t) = (V_m - \bar{V}) \cdot (t - t_s) \quad (18)$$

where $L_x(t)$ and $U_x(t)$ represent the upper and lower bound of the reachable domain $g_{12}(t)$ on the X-axis. For $\forall \tilde{X}(t) \in [L_x(t), U_x(t)]$, the upper boundary $U_y(t)$ and lower boundary $L_y(t)$ of the reachable domain $g_{12}(t)$ with Y-axis can be expressed as follows:

$$-L_y(t) = U_y(t) = \begin{cases} \sqrt{[V_m(t_t - t)]^2 - [\bar{V}(t_t - t) - \tilde{X}(t)]^2}, & \tilde{X}(t) < X_\alpha(t) \\ \sqrt{[V_m(t - t_s)]^2 - [\bar{V}(t - t_s) - \tilde{X}(t)]^2}, & \tilde{X}(t) \geq X_\alpha(t) \end{cases} \quad (19)$$

$$X_\alpha(t) = \frac{(V_m^2 + \bar{V}^2)(t_s + t_t - 2t)}{2\bar{V}} \quad (20)$$

Therefore, with the same principle of the X-axis coordinates, the probability density function of the Y-axis coordinates $Y(t)$ is subject to truncated normal distribution Pr_y :

$$Pr_y(Y(t) | \tilde{X}(t)) \sim \frac{N(0, \sigma_y^2(t))}{\phi(U_y(t)) - \phi(L_y(t))} \quad (21)$$

Variables $\sigma_x^2(t)$ and $\sigma_y^2(t)$ that appear in Equation 16 and Equation 21 donate the variance of truncated normal distribution in the X-axis and Y-axis directions of the reachable domain, respectively. The equations are as follows:

$$\sigma_x^2(t) = \sigma_y^2(t) = (V_m - \bar{V})^2 \cdot (t - t_s) \cdot (t_t - t) \quad (22)$$

3. AIRCRAFT CONFLICT DETECTION MODEL

The STP method is proposed to build the aircraft conflict scenario in this study, which combines with the flight plan of the aircraft in the TBO operating environment and the ETA information of a series of waypoints in the plan. In the STP model, the 4D trajectory of aircraft can be described as a spatiotemporal trajectory defined by a series of waypoints and their ETAs [33]. In this way, we transform the uncertain

4D trajectories of aircraft into determined spatiotemporal attainability domains, and the reachability of the aircraft on each flight segment is represented by STP. The necessary condition for conflict avoidance is that the STP of target aircraft should not intersect the protection domain of ownship. The overlapping area of the two spatiotemporal prisms constitutes the Potential Conflict Area (PCA), which reflects the space-time section of conflict probability.

Suppose that target aircraft B starts from point X_{B1} and makes a Brownian motion to point X_{B2} , its position at time t obeys the normal distribution within the reachable domain. On the flip side, the ownship A keeps a constant speed from x_{A1} to x_{A2} , and the protection domain is a circular area with a radius of r_A . The space-time prism formed by the two aircraft in the time quantum $t_\alpha = t_t - t_s$ is shown in Figure 4.

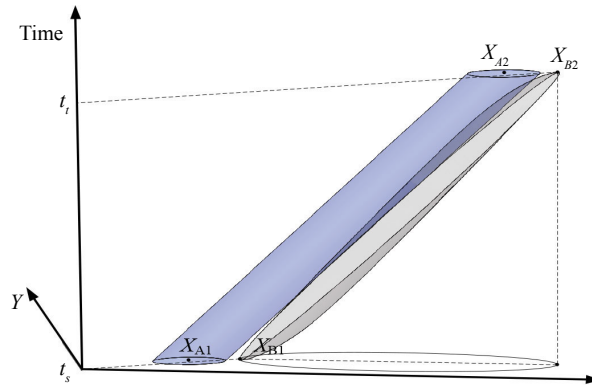


Figure 4 – The space-time prism paradigm for conflict scenarios

Figure 5 is the reachable domain profile of target aircraft, indicating the predicted positions of target aircraft at different times in the STP, during the time quantum t_α with a time distance of $1/7t_\alpha$.

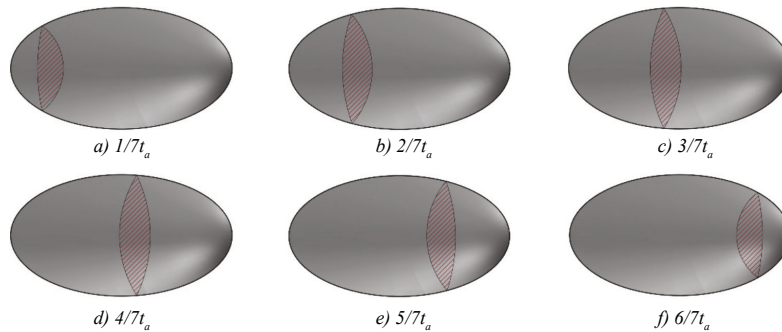


Figure 5 – Time based change of the traffic reachable domain

Figure 6 shows a potential conflict scenario between target aircraft B and ownship A. The red area represents the PCA for moment t ; x_A represents the position of ownship; U_x^P and L_x^P represent the upper and lower bound along X-axis, respectively; U_y^P and L_y^P represent the upper and lower boundaries of the PCA in

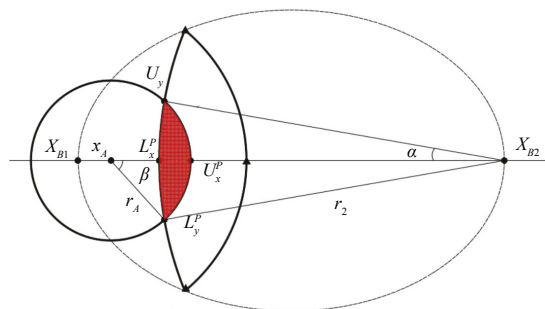


Figure 6 – Potential conflict for time t

the Y-axis direction, correspondingly.

The solution of intersection $U_y^P(u_x^P, u_y^P)$ and $L_y^P(l_x^P, l_y^P)$ is the same as that of $U_y(u_x, u_y)$ and $L_y(l_x, l_y)$ mentioned in the previous section. Furthermore, given the situation that the protection domain of the ownship completely comes within the reachable domain of target aircraft, the boundary point of the PCA at time t can be calculated as follows:

$$U_x^P = x_B + r_B \tag{23}$$

$$L_x^P = \begin{cases} x_2 - r_2, x_1 - r_1 \geq x_B - r_B \\ x_B - r_B, \frac{1}{2}(x_B + x_2, y_B + y_2) + \frac{r_B^2 - r_2^2}{2R_{12}^2}(x_2 - x_B, y_2 - y_B) + \end{cases} \tag{24}$$

$$U_y^P = \begin{cases} \frac{1}{2}\sqrt{2\frac{r_B^2 + r_2^2}{2R_{12}^2} - \frac{(r_B^2 - r_2^2)^2}{R_{12}^4}} - 1(y_2 - y_B, x_2 - x_B), u_y^P \geq y_B + r_B \\ (x_B, r_B), u_y^P \leq y_B + r_B \end{cases} \tag{25}$$

$$L_y^P = \begin{cases} \frac{1}{2}(x_B + x_2, y_B + y_2) + \frac{r_B^2 - r_2^2}{2R_{12}^2}(x_2 - x_B, y_2 - y_B) - \\ \frac{1}{2}\sqrt{2\frac{r_B^2 + r_2^2}{2R_{12}^2} - \frac{(r_B^2 - r_2^2)^2}{R_{12}^4}} - 1(y_2 - y_B, x_2 - x_B), l_y^P \leq y_B - r_B \\ (x_B, y_B - r_B), l_y^P \geq y_B - r_B \end{cases} \tag{26}$$

And then, the instantaneous conflict probability P_B between target aircraft and ownship at time t is denoted as follows:

$$P_B = \int_{L_x^P}^{U_x^P} \int_{L_y^P}^{U_y^P} Pr(X(t))Pr(Y(t)) dx dy \tag{27}$$

Consequently, the total conflict probability P between the two aircraft in the time interval t_α can be written as follows:

$$P = \int_{t_s}^{t_f} P_B dt \tag{28}$$

4. OPTIMAL DISTANCE CONTROL STRATEGY

In the previous section, we have calculated the total conflict probability P between the ownship A and the target aircraft B. For civil aviation, it is considered that when the total conflict probability $P \geq 1 \cdot 10^{-7}$, the flight path of the aircraft needs to be re-planned to ensure flight safety, which means controlling the separation between the two aircraft within the safe range, so as to avoid flight conflict. In this section, therefore, based on the previous section 3, a spacing maintenance method is proposed for aircraft judged to be in potential conflict. The purpose of this method is to plan a conflict-free trajectory without changing the flight plan of the target aircraft while allowing the aircraft to make minimal manoeuvres.

As a rising evolutionary algorithm, the PSO algorithm has obvious advantages in solving problems whose objective functions are nonlinear and non-convex [34]. Distinct from other intelligent optimisation algorithms, the PSO algorithm aims to find the optimal solution through the cooperation of individuals. Each particle is given a random speed and flows in the whole problem space, and the evolution of particles is realised by the cooperation and competition between particles. The parallel computing function of the PSO algorithm makes it prone to obtaining a better computing result with lower computing costs, it also has the drawback of being susceptible to local optimal solutions [35]. Because of this, the LPSO algorithm somewhat enhances the local optimum problem by converting the constant PSO coefficients to linear functions, but it is challenging to balance the capabilities of global and local search in the late convergence stage. In this section, the velocity update constant of the particle swarm was nonlinearly optimised to enhance the algorithm's ability to perform global searches while preventing the algorithm from entering a local optimum as a result of a decrease in particle diversity at the algorithm's late convergence stage. The description of the

advanced particle swarm optimisation algorithm is as follows:

Suppose a two-dimensional space with a particle swarm size of Z , and perform n th update iterations. The position and velocity of a single particle can be expressed as $X=(x_x, x_y, x_t)$ and $V=(v_x, v_y, v_t)$. The standard update formula [25, 29] for the position and velocity of this particle are given as follows:

$$x_{k+1} = x_k + v_{k+1} \cdot \frac{T}{n} \tag{29}$$

$$v_{k+1} = wv_k + c_1 r_1 (pBest - x_k) + c_2 r_2 (gBest - x_k) \tag{30}$$

In Equation 29, w represents the inertia weight constant; the global acceleration constant is represented by c_1 ; the local acceleration constant is represented by c_2 ; r_1 and r_2 is a random number between (0,1); T represents the time step of algorithm calculation.

Set the coordinates of the starting point of the ownship as $X_{A1}(x_1, y_1, T_1)$ and the end point coordinate as $X_{A2}(x_n, y_n, T_n)$; the coordinates of the starting point of the aircraft as $X_{B1}(x'_1, y'_1, T_1)$, and the end point coordinates as $X_{B2}(x'_n, y'_n, T_n)$. Then the path of a single particle along the X-axis and Y-axis directions can be indicated as n-dimensional vectors $X=(x'_1, x'_2, \dots, x'_n)$ and $Y=(y'_1, y'_2, \dots, y'_n)$, respectively. Equations 30–32 are the constraint on velocity and position update.

$$\begin{cases} \sqrt{(x_k - x_1)^2 + (y_k - y_1)^2} \leq k \frac{v_{max} T}{n} \\ \sqrt{(x_k - x_1)^2 + (y_k - y_1)^2} \geq (n - k) \frac{v_{max} T}{n} \end{cases} \tag{31}$$

$$\begin{cases} v_{k+1} = v_{max}, & \text{if } v_k > v_{max} \\ v_{k+1} = v_{min}, & \text{if } v_k < v_{min} \end{cases} \tag{32}$$

In present work, the inertia weight constants and acceleration constants in Equation 29 are replaced by nonlinear functions which are related to the number of iteration steps, i.e. the algorithm is matched with more suitable weight values at different stages of the iteration. In comparison to the optimisation method with linear weights, the nonlinear function can make the algorithm gain the ability to find the optimal point in a larger range by setting a larger search speed and inertia weights in the early stage of convergence; and enhance the local search ability of the algorithm by reducing the search speed and inertia weights in the late stage of convergence. This can balance the algorithm’s global search ability and local search ability. The expressions are as follows:

$$w(k) = \frac{w_{max} - w_{min}}{2} \cos\left(\pi \frac{k}{n}\right) + \frac{w_{max} + w_{min}}{2} \tag{33}$$

$$c_1(k) = \frac{c_{1,max} - c_{1,min}}{2} \sin\left(\frac{\pi}{2} \frac{n - k}{n}\right) + \frac{c_{1,max} + c_{1,min}}{2} \tag{34}$$

$$c_2(k) = \frac{c_{2,max} - c_{2,min}}{2} \sin\left(\frac{\pi}{2} \frac{k - n}{n}\right) + \frac{c_{2,max} + c_{2,min}}{2} \tag{35}$$

where k represents the current iteration. According to [36], when w takes a value of [0.4,0.95], c_1 and c_2 take a value of [0.5,2.5], we can get a higher optimisation effect. For this reason, we determine that $w_{max}=0.95$, $w_{min}=0.4$; $c_{1,max}$ and $c_{2,max}$ are taken as 2.5, $c_{1,min}$ and $c_{2,min}$ are taken as 0.5. Then the updated formula of particle velocity is rewritten as follows:

$$v_{k+1} = w(k)v_k + c_1(k)r_1(pBest - x_k) + c_2(k)r_2(gBest - x_k) \tag{36}$$

In this section, the ownship was optimised to do the minimum manoeuvre in the separation adjustment time, which means the change of the speed vector of the ownship is controlled to be the smallest. Form the previous description, it can be seen that if the ownship keeps a constant speed, the trajectory should be a straight-line segment in problem space. Therefore, the smaller the deviation of the optimised trajectory from the straight segment, the smaller the control amount of the speed vector by the aircraft. Suppose that the fitness function f is the minimum control amount of the ownship’s speed vector in time quantum T .

$$f = \min \left\{ \sum_{k=1}^n \left(\sqrt{(x_{k+1} - x_k)^2 + (y_{k+1} - y_k)^2} \mu(v_{k+1} - v_k) \right) \right\} \tag{37}$$

where μ is a penalty term which indicates the incremental constraint for speed update. The pseudo code of the NPSO algorithm is displayed below:

```

procedure NPSO
  for each particle  $i$ 
    Initialise velocity  $V_i$  and position  $X_i$  for particle  $i$ 
    Evaluate particle  $i$  and set  $pBest_i = X_i$ 
  end for
   $gBest = \min\{pBest_i\}$ 
  while not stop
    for  $i=1$  to  $N$ 
      Update the velocity and position of particle  $i$ 
      Evaluate particle  $i$ 
      if  $f(X_i) < f(pBest_i)$ 
         $pBest_i = X_i$ 
        if  $f(pBest_i) < f(X_i)$ 
           $gBest = pBest_i$ 
        end if
      end if
    end for
  end while
  print  $gBest$ 
end procedure
    
```

5. SIMULATION CASE

5.1 Simulation of the total conflict probability

According to the calculation of conflict probability which was introduced in section 3, the total conflict probability between two aircraft is influenced by two factors: the area of the PCA and the degree of deviation of the PCA from the centreline of the other aircraft’s reachable domain. Consequently, this section summarises the influencing factors of the total conflict probability as: the initial speed of the ownship, the initial distance between the two aircrafts and the length of the conflicting flight segment.

All simulations in this study were run in MATLAB 2017b with the Windows 10 (64bit) operating system, and the computer hardware configuration used was AMD Ryzen 3 2200G CPU and Radeon Vega Graphics. The Airbus A320 model was used as an example in both the ownship and target aircraft addressed in this study. Considering the flight state and air control constraints of the aircraft during the actual flight process according to the BADA document, the initial state parameters and external environment parameters of the two aircraft were selected as shown in Table 1. Figure 7 depicts the time-dependent instantaneous conflict probability curves for the initial parameters in Table 1.

Figure 7 depicts the three phases that the local protected area goes through from the moment it enters the reachable domain of the target aircraft to the time it leaves. Firstly, at $t=0.05$ h, the ownship protection zone starts to engage in the reachable domain of target aircraft; at $t=0.107$ h the instantaneous conflict probability

Table 1 – Advanced particle swarm optimisation algorithm

Parameter	Value
Initial speed of target aircraft V_0^B [km/h]	750
Initial speed of ownship V_0^A [km/h]	850
Initial distance between two aircrafts X_0 [km]	40
Heading angle variation range θ [°]	[-30,30]
Velocity range of airspeed V [m/s]	[850±100]
Length of conflicting flight segment D [km]	150
Radius of protection domain r [km]	10

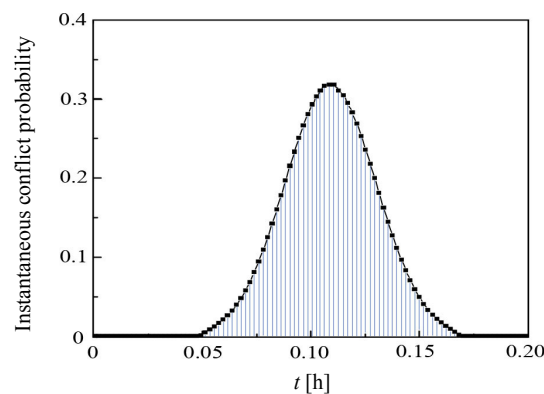


Figure 7 – Variation of instantaneous conflict probability with time

reaches a maximum; at $t=0.169$ h, the ownship is completely disengaged from the reachable domain, accompanied with the probability density of the conflict deduced to zero.

By changing the values of the initial state parameters and calculating the corresponding total conflict probability within a time interval t_{α} , the curve of total conflict probability with the change of initial state can be plotted. The logic of the conflict detection model in this study is validated by analysing the trend of the total conflict probability with the initial state parameters. Three sets of conflict scenarios are constructed in this section based on two parameters that influence the total conflict probability:

- 1) Keep the parameters of target aircraft unchanged and only change the initial speed of ownship.
- 2) Keep the parameters of the two aircraft unchanged and change the initial distance between the two aircrafts.
- 3) Keep the parameters of the two aircraft unchanged and change the length of the conflicting flight segment.

Figure 8 describes the change trend of the whole conflict probability when the initial speed ($V_0^A=800,825,850,875,900$ km/h) of the ownship is changed while the rest of the initial parameters are maintained. It can be seen that the initial velocity of the ownship is positively correlated with the total conflict probability. And without changing other parameters, with the gradual increase of the initial speed of the machine, the possibility of conflict between the two aircrafts is also rising in tandem, which is consistent with the objective law that the probability of conflict increases with the relative speed of the two aircraft.

The influence of the initial separation ($X_0=30,40,50,60,70$ km) between the two aircrafts on the total conflict probability is shown in Figure 8b. The Figure shows that the initial separation between two aircrafts is negatively correlated with the total conflict probability, which is consistent with the objective law that the probability of conflict decreases as the initial relative position of the two aircraft increases. Furthermore, a safe initial distance can be obtained, which enables the aircraft to maintain a conflict-free and safe flight in the current flight state. According to the initial parameters selected in this study, when $X_0=70$ km, the total conflict probability is reduced to 0.

Figure 8c describes the impact curve of the conflict segment length on the total conflict probability. It is easy to find from Figure 10 that the length of the leg is positively correlated with the total conflict probability, which is consistent with the assumption that the longer the interval between waypoints, the greater the uncertainty of aircraft conflict. The impact of the target aircraft's flight intentions on the ownship increases enormously, since the leg distance increases, and the increase trend is particularly obvious after the leg distance exceeds 125 km. In addition, the influence of leg distance on the total conflict probability is not very significant, compared to the factors mentioned above.

The above simulation results show that the conflict detection model assumptions proposed in this study are compatible with objective laws in actual aircraft cruise missions. In addition, in the next section we will mainly design cases based on the ownship's speed and initial position, and study the separation control strategy.

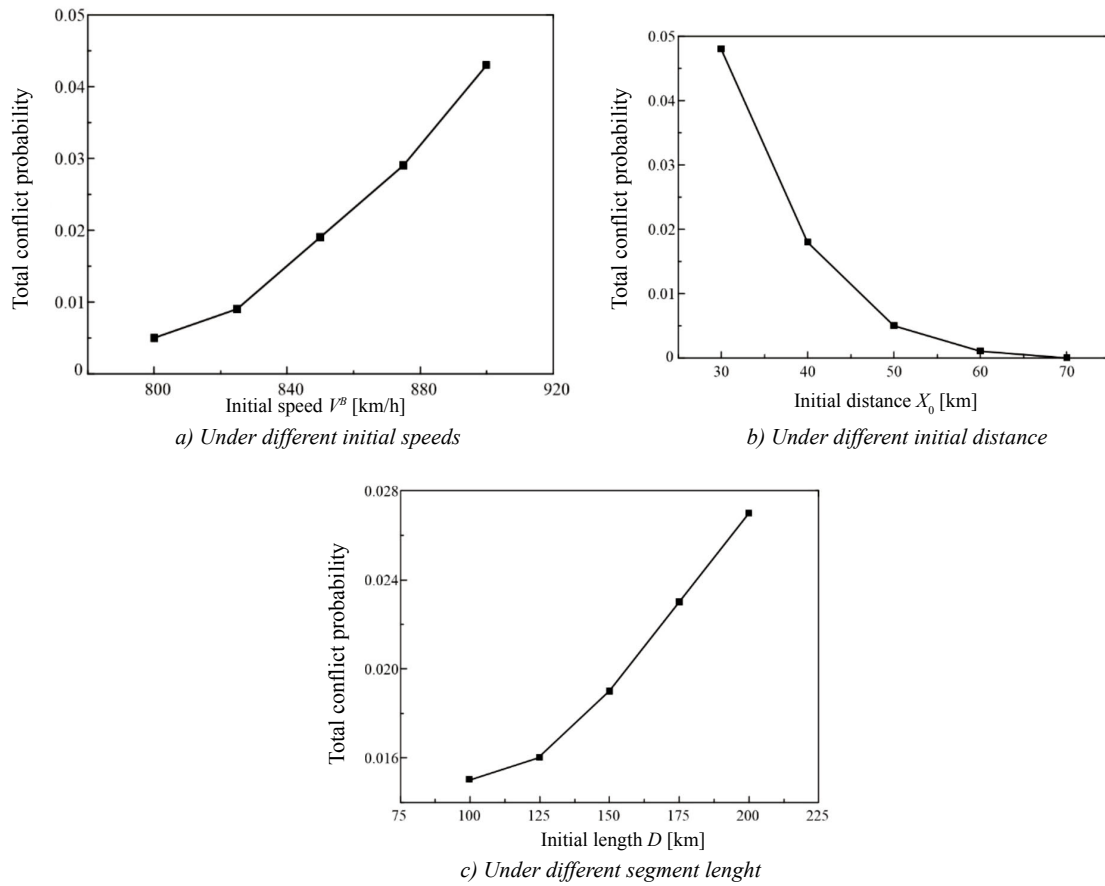


Figure 8 – Variation of the total conflict probability

5.2 Separation control algorithm superiority analysis

To verify the effectiveness of the improved NPSO algorithm based on nonlinearity in this study, the data in Table 1 and Table 2 were used for the numerical simulation of the NPSO algorithm. At the same time, we set up horizontal and vertical comparison simulation, i.e. the NPSO is compared with the traditional PSO algorithm and the LPSO algorithm, which is based on the improved linearisation method. The simulation results are shown in Figure 9 and Table 3.

Table 2 – Supplement of simulation parameters

Parameter	Value
Initial point coordinates	(30,20,0)
End point coordinates	(47,20, 60)
Particle swarm size Z	100
Maximum iterations n	500
Inertia weights w	[0.4, 0.95]
Global acceleration $C1$	[0.5, 2.5]
Local acceleration $C2$	[0.5, 2.5]

Figure 9 shows the free-conflict trajectory of the ownship from the initial point to the end point in time quantum t_{α} , which was calculated by the traditional PSO and the improved LPSO and NPSO algorithms, respectively. The white square dot in Figure 9 represents the initial point of the ownship trajectory, the black dot represents the end point of the ownship trajectory and the black solid lines represent the ownship trajectories. Orange, purple and red columns are the ownship protection zone of PSO, LPSO and NPSO algorithms, respectively. Table 3 shows the comparison of numerical calculation results of the three algorithms.

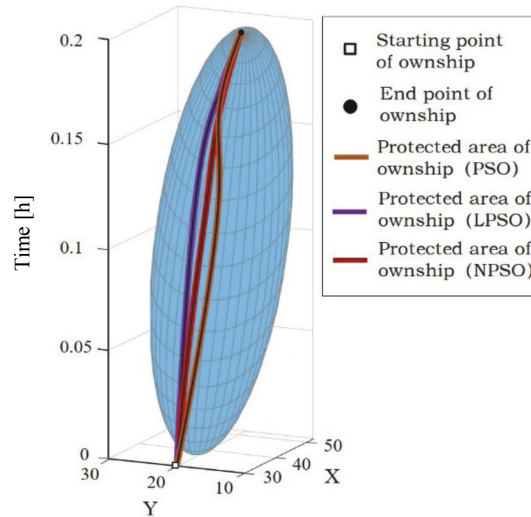


Figure 9 – Comparison of optimal separation trajectory curves

Table 3 – Comparison of numerical calculation results

Optimisation algorithm	Optimum value	Maximum speed change [km/h]	Time cost [s]
PSO	73.21	62.94	4.36
LPSO	66.35	56.03	4.76
NPSO	62.32	50.45	5.69

As can be interpreted in Table 3, the NPSO algorithm proposed in this study improved the optimal value by 14.88% compared to the conventional PSO algorithm and 6.46% compared to the LPSO algorithm with a slight increase in computational cost. In terms of the maximum speed change, the NPSO algorithm outperforms the LPSO algorithm by 9.96% and the conventional PSO algorithm by 19.84%. The simulation findings mentioned above demonstrate that the NPSO algorithm, which is based on non-linear adaptive functions, more effectively addresses numerical problems compared to traditional PSO methods and the LPSO algorithm. Therefore, this study adopts the NPSO algorithm to ascertain the optimal spacing configuration strategy for conflicting aircrafts.

5.3 NPSO-based optimal separation configuration

In this research, six conflict scenarios are simulated using the two influencing elements of initial speed and initial distance, and the impact of varied initial status parameters on the optimal separation control method is investigated. Figures 10 and 11 show the optimal separation trajectory curves of the ownship’s trajectory without conflict with target aircraft’s STP for different initial speed conditions. The local protective zone is masked in the figure for ease of observation and only the trajectory curve of the local aircraft is preserved.

This study employs a combination of heading and speed adjustments to achieve optimal separation configuration for the ownship. Figure 11 depicts the variation curves of heading angle and speed for three sets of optimal separation configuration strategies. When the initial speed of the ownship is slightly different from that of the target aircraft ($V_0^A=800$ km/h, $V_0^B=750$ km/h), then only minor speed adjustments are required to ensure a safe separation from the target aircraft’s STP. The trend of the heading angle and speed curves reveals that as the initial speed of the aircraft increases, the corresponding spacing configuration strategy becomes more aggressive, necessitating larger heading angles and speeds to adjust the aircraft’s position. When $V_0^A=900$ km/h, the aircraft ceases deceleration after reaching the lower limit of the set speed. The variation curves demonstrate that, under different initial speeds, neither the heading nor speed adjustment values exceed the set range, thus confirming the rationality of the separation configuration strategy proposed in this study.

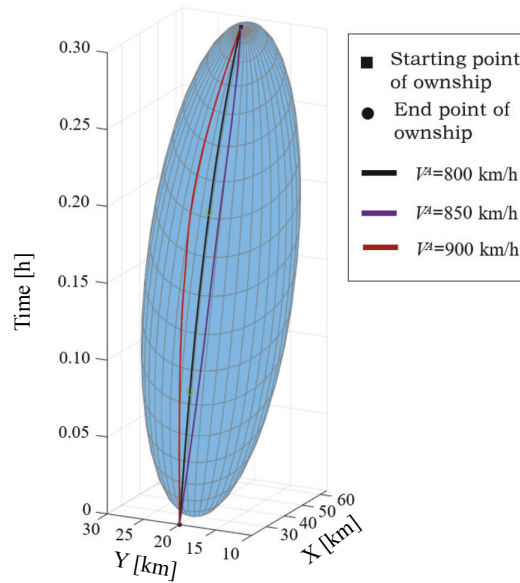


Figure 10 – Curves of the optimal separation trajectory for ownship

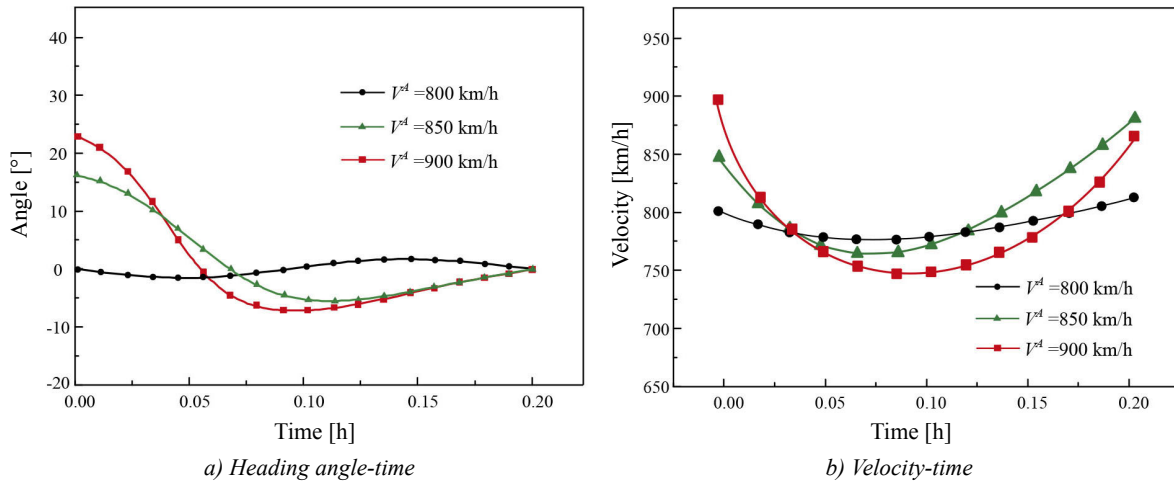


Figure 11 – Variation curves of heading angle and velocity under different initial speeds

The simulation results of the separation between the local machine and STP changes with time are shown in Figure 12. The simulation results demonstrate that the minimum separation between the local machine and the STP is reached in all three sets of conflict scenarios with initial speeds. The difference between the three sets of conflicts is that the separation between the ownship and STP with larger speed maintains at the minimum separation for a longer time.

Through comprehensive analysis of optimisation results for heading angle, velocity and spacing under different initial velocity conditions, this study demonstrates the effectiveness of the NPSO algorithm in avoiding conflicts and reconfiguring optimal safety separation for the aircraft. In addition, to investigate the influence of the initial distance between the aircraft and the target aircraft on the separation configuration strategy of the NPSO algorithm, numerical simulations were conducted on conflict scenarios characterised by three disparate initial distances.

To investigate the impact of the initial distance between the ownship and the target aircraft on the separation control strategy, three sets of conflict scenarios with the initial distance are numerically simulated in this study, and the simulation results are displayed in Figures 13 and 14.

The optimal heading and velocity allocation strategies for the ownship under different initial distance

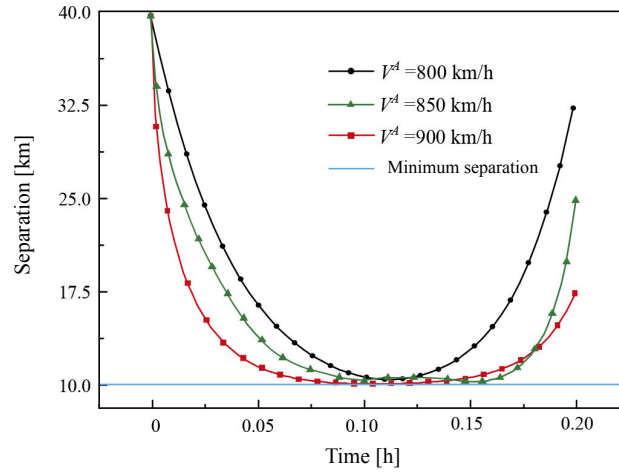


Figure 12 – Separation-time curves under different initial speeds

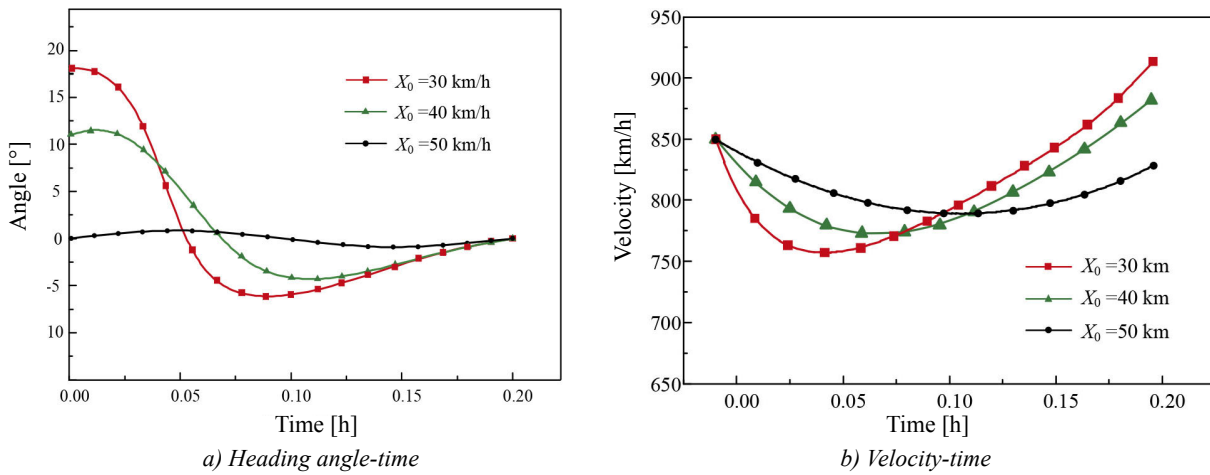


Figure 13 – Variation curves of heading angle and velocity under different initial distances

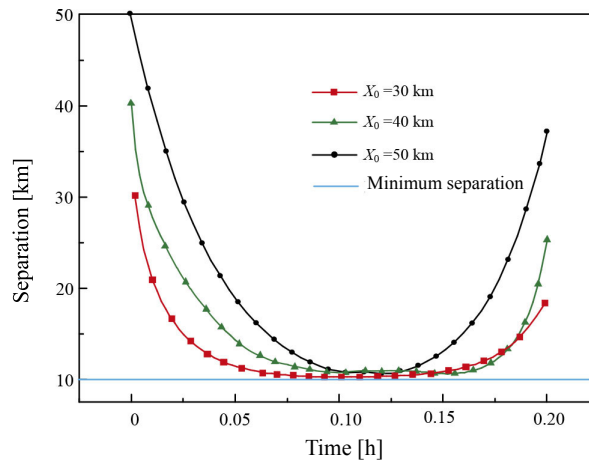


Figure 14 – Separation-time curves under different initial distances

conditions are illustrated in *Figure 13*. The simulation results indicate that as the initial distance decreases, the trajectory configuration strategies adopt larger heading angle and greater velocity adjustment to avoid conflict with the target’s STP. The simulation results for the three sets of initial distances consistently maintain the heading angles and velocities within the prescribed bounds, thereby corroborating the efficacy of the spacing configuration algorithm. Furthermore, *Figure 14* demonstrates that the NPSO optimisation algorithm

proposed in this study guarantees a safe separation distance between ownship and the target's STP under various initial distance scenarios, thereby confirming the rationality of the algorithm.

6. CONCLUSION

In this study, we addressed the issue of following conflict scenarios arising from the uncertain flight status of cruise aircraft during the pre-tactical phase, proposed a conflict detection model to identify potential conflict threats and utilised the NPSO optimisation algorithm to reconfigure the separation between conflicting aircraft.

- 1) To enhance the safety of aircraft flying in four-dimensional flight segments with incomplete information, a total conflict detection model based on truncated normal distribution was proposed. This model converts the target aircraft's uncertain flight trajectory due to unknown intention into a reachable domain and analyses the key variables influencing the total conflict probability by computing the probability density function of potential conflict areas.
- 2) By comparing the computational results of several commonly used optimisation algorithms, we ultimately employ the NPSO algorithm to determine the optimal spacing configuration strategy for resolving conflicts among aircraft. This strategy involves reassigning the spacing between conflicting aircraft through a combination of heading and speed allocation schemes. The results demonstrate that our algorithm effectively eliminates the potential flight conflicts arising from uncertain states.
- 3) The simulation results show that the NPSO algorithm improved the optimal value by 14.88% when compared to the conventional PSO and 6.46% when compared to the linear PSO. It also reduced the optimal value's maximum speed fluctuation by 19.84% and made it better by 9.96% when compared to the linear PSO. Additionally, the separation control requirements can be satisfied by the NPSO algorithm in a variety of initial parameter situations.

ACKNOWLEDGEMENT

This research was funded by the Major Project of the National Social Science Fund of China (grant no. 61773202); the National Social Science Fund of China (grant no. 52072174); the National Key R&D Plan (grant no. 2021YFB1600500); Civil Aviation General Aviation Operation Key Laboratory of China Civil Aviation Management Cadre Institute (grant no. 6142505180407); National Defence Science and Technology Key Laboratory of Avionics System Integrated Technology of China Institute of Aeronautical Radio Electronics (grant no. CAMICKFJJ-2019-04).

REFERENCES

- [1] Gomez Comendador VF, Arnaldo Valdés RM, Sanchez Cidoncha M. Impact of trajectories' uncertainty in existing ATC complexity methodologies and metrics for DAC and FCA SESAR concepts. *Energies*. 2019;12(8):1-25. DOI: 10.3390/en12081559.
- [2] Hao SQ, Cheng SW, Zhang YP. A multi-aircraft conflict detection and resolution method for 4-dimensional trajectory-based operation. *Chinese Journal of Aeronautics*. 2018;7(148):177-191. DOI: 10.1016/j.cja.2018.04.017.
- [3] Jacquemart D, Morio J. Adaptive interacting particle system algorithm for aircraft conflict probability estimation. *Aerospace Science & Technology*. 2016;7(55):431-438. DOI: 10.1016/j.ast.2016.05.027.
- [4] Han D, et al. A conflict detection algorithm for low-altitude flights based on SVM. *Journal of Beijing University of Aeronautics and Astronautics*. 2018;3(44):576-582. DOI: 10.13700/j.bh.1001-5965.2017.0159.
- [5] Wu MG, Wang ZK, Wen XX. Aircraft conflict resolution model based on geometric optimization. *Systems Engineering and Electronics*. 2019;41(4):863-869. DOI: 10.3969/j.issn.1001-506X.2019.04.23.
- [6] Sun MH, Rand K, Fleming C. 4 Dimensional waypoint generation for conflict-free trajectory based operation. *Aerospace Science and Technology*. 2019;88:350-361. DOI: 10.1016/j.ast.2019.03.035.
- [7] Guan X, et al. A strategic flight conflict avoidance approach based on a memetic algorithm. *Chinese Journal of Aeronautics*. 2014;1(27):863-869. DOI: 10.1016/j.cja.2013.12.002.
- [8] Hernandez-Romero E, Valenzuela A, Rivas D. A probabilistic approach to measure aircraft conflict severity considering wind forecast uncertainty. *Aerospace Science and Technology*. 2019;86:401-414. DOI:

- 10.1016/j.ast.2019.01.024.
- [9] Russell AP, Heinz E. Conflict probability estimation generalized to non-level flight. *Journal of Guidance, Control, and Dynamics*. 1997;3(7):588-596. DOI: 10.2514/atcq.7.3.195.
- [10] Lambert A, Gruyer D, Pierre GS. A fast monte carlo algorithm for collision probability estimation. *International Conference on Control, 17-20 Dec. 2008, San Antonio, USA*. 2014. p. 406-411. DOI: 10.1109/ICARCV.2008.4795553.
- [11] Liu Y, et al. Short-term conflict detection algorithm for free flight in low-altitude airspace. *Journal of Beijing University of Aeronautics and Astronautics*. 2017;43(9):1873-1881. DOI: 10.13700/j.bh.1001-5965.2016.0687.
- [12] Alizadeh A, Uzun M, Koyuncu E. Optimal en-route trajectory planning based on wind information. *IFC*. 2018;51(9):180-185. DOI: 10.1016/j.ifacol.2018.07.030.
- [13] Lucas BM, Vitor FR, Cristiano PG. 4D trajectory conflict detection and resolution using decision tree pruning method. *IEEE Latin America Transactions*. 2023;21(2):277-287. DOI: 10.1109/TLA.2023.10015220.
- [14] Liu ZA, Xiao G, Mao JZ. A framework for strategic online en-route operations: Integrating traffic flow and strategic conflict managements. *Transportation Research Part C*. 2023;147:103996. DOI: 10.1016/j.trc.2022.103996.
- [15] Zhang JF, Jiang HX, Wu XG. 4D trajectory prediction based on BADA and aircraft intent. *Journal of Southwest Jiaotong University*. 2014;49(3):1873-1881. DOI: 10.3969/j.issn.0258-2724.2014.03.028.
- [16] Vito VD, Torrano G. Fast-time numerical validation of an ADS-B based automatic separation assurance and collision avoidance system. *Integrated Communications Navigation and Surveillance Conference (ICNS), 20-22 Apr, Dulles, USA*. 2021.
- [17] Ni YD, Liu P, Ma SY. An improved trajectory prediction algorithm based on ADS-B intent information. *Telecommunication Engineering*. 2014;43(9). DOI: 10.3969/j.issn.1001-893x.2014.02.008.
- [18] Zhang K, et al. Bayesian trajectory prediction for a hypersonic gliding geentry vehicle based on intent inference. *Journal of Astronautics*. 2018;39(11):1258-1265. DOI: 10.3873/j.issn.1000-1328.2018.11.008.
- [19] Hao SQ, Zhang YP, Cheng SW. Probabilistic multi-aircraft conflict detection approach for trajectory based operation. *Transportation Research: Part C*. 2018;95(0):698-712. DOI: 10.1016/j.trc.2018.08.010.
- [20] Shi L, Wu RB, Huang XX. Conflict detection algorithm based on overall conflict probability and three-dimensional brownian motion. *Journal of Electronics & Information Technology*. 2015;37(2):360-366. DOI: 10.11999/JEIT140363.
- [21] Song Y, Miller HJ. Simulating visit probability distributions within planar space-time prisms. *International Journal of Geographical Information Science*. 2014;28(1):104-125. DOI: 10.1080/13658816.2013.830308.
- [22] Chen YT, et al. Autonomous trajectory planning and conflict management technology in restricted airspace. *Acta Aeronautica et Astronautica Sinica*. 2020;41(9):324045. DOI: 10.7527/S1000-6893.2020.24045.
- [23] Shiri H, Park J, Bennis M. Remote UAV online path planning via neural network based opportunistic control. *IEEE Wireless Communication Letters*. 2020;9(6):861-865. DOI: 10.1109/LWC.2020.2973624.
- [24] Meng G, Fei Q. Flight conflict resolution for civil aviation based on ant colony optimization. *6th International Symposium on Computational Intelligence & Design, 28-29 Oct, Hangzhou, China*. 2012.
- [25] Gao Y, Zhang XJ, Guan XM. Cooperative multi-aircraft conflict resolution based on co-evolution. *International Symposium on Instrumentation & Measurement, 25-28 Aug, Sanya, China*. 2012.
- [26] Shao SK, Yu P, He CL. Efficient path planning for UAV formation via comprehensively improved particle swarm optimization. *ISA Transactions*. 2020;97:415-430. DOI: 10.1016/j.isatra.2019.08.018.
- [27] Omer J, Farges JL. Hybridization of nonlinear and mixed-integer linear programming for aircraft separation with trajectory recovery. *IEEE Transactions on Intelligent Transportation Systems*. 2013;14(3):1218-1230.
- [28] Dias F, Hijazi H, Rey D. Disjunctive linear separation conditions and mixed-integer formulations for aircraft conflict resolution. *European Journal of Operational Research*. 2022;296:520-538. DOI: 10.1016/j.ejor.2021.03.059.
- [29] Matsuno Y, et al. Stochastic optimal control for aircraft conflict resolution under wind uncertainty. *ISA Transactions*. 2015;43:77-88. DOI: 10.1016/j.ast.2015.02.018.
- [30] Emami H, Derakhshan F. Multi-agent based solution for free flight conflict detection and resolution using particle swarm optimization algorithm. *UPB Scientific Bulletin, Series C: Electrical Engineering and Computer Science*. 2014;3(76):49-64.

- [31] Lu XL, He G. QPSO algorithm based on Lévy flight and its application in fuzzy portfolio. *Applied Soft Computing*. 2021;1(99):106894. DOI: 10.1016/j.asoc.2020.106894.
- [32] Lauderdale TA, et al. Separation at crossing waypoints under wind uncertainty in urban air mobility. *AIAA Aviation 2021 Forum, 02 Aug, Hangzhou, China*. 2021. DOI: 10.2514/6.2021-2351.
- [33] Yu H. A direction-constrained space-time prism-based approach for quantifying possible multi-ship collision risks. *IEEE Transactions on Intelligent Transportation Systems*. 2019;1(22):131-141. DOI: 10.1109/TITS.2019.2955048.
- [34] Malaek SM, Golachoubian M. Enhanced conflict resolution manoeuvres for dense airspaces. *IEEE Transactions on Aerospace and Electronic Systems*. 2019;5(56):131-141. DOI: 10.1109/TAES.2020.2972422.
- [35] Han S. Industrial robot trajectory planning based on improved PSO algorithm. *Journal of Physics Conference Series*. 2021;1(1820):012185. DOI: 10.1088/1742-6596/1820/1/012185.
- [36] Wu GC. *Research on path planning based on particles warm optimization*. PhD thesis. Yanshan University; 2016.

任宣铭 博士, 汤新民 博士 (通讯作者), 张康 博士, 鲁其兴 博士
基于不确定飞行轨迹的冲突检测与间隔配置方法

摘要

针对预战术阶段的双机冲突情景, 通过将目标飞机的不确定飞行航迹转化为航空器性能约束下的时空轨迹, 提出了一种基于截断正态分布的冲突检测模型, 并通过数值模拟分析了影响总冲突概率的影响因素。对于冲突情景, 应用非线性粒子群优化(NPSO)算法来求解本机的最优间隔配置策略。仿真结果表明, 相比于传统的PSO算法, 改进的NPSO算法最优值提高了14.88%, 并且最大速度变化量降低了19.84%。同时仿真也表明算法能够在不同初始参数下保持最小间隔要求, 证明了其具有比较强的适应性。

关键字

冲突检测; 间隔配置; 时空轨迹; 飞行轨迹不确定; 非线性粒子群优化。